Magnetoresistance in inhomogeneous graphene/metal hybrids

Zakaria Moktadir and Hiroshi Mizuta

Citation: J. Appl. Phys. **113**, 083907 (2013); doi: 10.1063/1.4793647
View online: http://dx.doi.org/10.1063/1.4793647
View Table of Contents: http://jap.aip.org/resource/1/JAPIAU/v113/i8
Published by the American Institute of Physics.

JOURNAL OF APPLIED PHYSICS **113**, 083907 (2013)

Magnetoresistance in inhomogeneous graphene/metal hybrids

Zakaria Moktadir[1,a)] and Hiroshi Mizuta[1,2]
[1]*Electronics and Computer Science, Faculty of Applied Physical Sciences, Southampton University, Southampton, United Kingdom*
[2]*School of Materials Science, JAIST, Nomi, Ishikawa 923-1292, Japan*

(Received 23 November 2012; accepted 13 February 2013; published online 27 February 2013)

We investigate extraordinary magnetoresistance (EMR) of inhomogeneous graphene-metal hybrids using finite element modelling. Inhomogeneous graphene is a binary system made of electron and hole puddles. Two geometries of the embedded metallic structure were considered: circular and fishbone geometries. We found that the breaking of graphene into charge puddles weakens the magnetoresistance of the hybrid system compared to a homogeneous graphene-metal system. For a fixed value of the magnetic field, the magnetoresistance increases with decreasing area fraction occupied by electrons puddles. Fishbone geometry showed an enhanced magnetoresistance compared to circular geometry. The EMR is also investigated as a function of the contact resistance for the fishbone geometry where it was found that a minimal contact resistance is essential to obtain enhanced EMR in graphene-metal hybrid devices. © *2013 American Institute of Physics*. [http://dx.doi.org/10.1063/1.4793647]

I. INTRODUCTION

Graphene has recently attracted a huge amount of interest, thanks to its remarkable electrical and mechanical attributes. Graphene is a two-dimensional material where carbon atoms are arranged in a honeycomb structure. This atomic arrangement gives graphene its specific band structure where the energy dispersion is linear near $\mathbf{K}$ and $\mathbf{K}'$ in the Brillouin's zone, i.e., $E = \hbar v_F|\mathbf{k}|$, where $v_F \simeq 10^6\,\mathrm{m\,s^{-1}}$. At $T = 0$, the Fermi level of graphene E_F separates the valence and the conduction bands exactly at the Dirac point. The density of states in the vicinity of the Dirac point is linear in energy, giving electrons in graphene their massless character of Dirac fermions.

A remarkable feature of graphene is that it shows a minimum value of the conductivity σ_{min} in the order of few e^2/h.[1–3] Work related to the occurrence of σ_{min} was carried out by several authors stating it is either due to rippling in graphene[4,5] or due to short range disorder.[6,7] In fact, it is widely acceptable that the decomposition of graphene into electrons and holes puddles near the neutrality point is caused by fluctuations of the potential originating from charge impurities residing in the underlying substrate. A self-consistent theory of graphene transport at low densities was developed by Adam *et al.*,[8] where the graphene puddle density is derived from the potential and density fluctuations caused by the charged impurities. The presence of electrons and holes puddles in graphene was first experimentally demonstrated by Martin *et al.*[9] using a single electron transistor. Chen *et al.*[10] carried out experimental observations stating that σ_{min} is not governed by the physics of the Dirac point singularity, but by carrier-density inhomogeneity induced by the potential of charged impurities. In other related work, Cho and Fuhrer[3] investigated the magnetic field-dependent longitudinal and Hall resistivities ρ_{xx} and ρ_{xy}, near the neutrality point. They found that at charge densities near σ_{min}, ρ_{xx} is strongly enhanced whilst ρ_{xy} vanished, meaning that electrons and holes contribute equally to the current in an inhomogeneous graphene sheet. Their observations are inconsistent with the standard two-fluid model[11] but consistent with the prediction for inhomogeneously distributed electron and hole regions of equal mobility.

It is well known that the inclusion of metallic embedded structures in narrow gap, high mobility thin film semiconductors allows a significant enhancement of the magnetoresistance.[12–14] It is therefore natural to consider graphene for this type of magnetic sensors. In addition, as graphene is easily gated, it allows device sensitivity tuning and compensation for the variability of device properties during the fabrication process.[15,16] This type of devices made of graphene/Au hybrids were recently experimentally demonstrated.[15,17]

The purpose of this work is to investigate the extraordinary magnetoresistance (EMR) in inhomogeneous graphene with embedded metallic inclusions. We show quantitatively using finite element modelling (FEM) that the presence of n-type and p-type puddles imply significant change in magnetoresistance properties of graphene-metal hybrid systems. The effect of graphene-metal contact resistance is also considered.

II. EFFECTIVE CONDUCTIVITY IN INHOMOGENEOUS GRAPHENE

Here, we will use the effective-medium approximation (EMA) model[18] for the magnetoresistance and Hall coefficients of graphene subjected to a perpendicular magnetic field $\mathbf{B} = B\mathbf{z}$, where $\mathbf{z}$ is the unit vector in the z-direction. The graphene sheet is considered as a binary system made of n-type and p-type puddles with area fraction f_n and $f_p = 1 - f_n$, respectively. In addition, the area of puddles is much larger than the carrier mean free path so that it can be described by its own magnetoconductivity tensor σ_n for n-type puddles

a)Electronic mail: zm@ecs.soton.ac.uk.

and σ_p for p-type puddles.[18] In the presence of a magnetic field, the conductivity tensors are given by

$$\sigma_n = \sigma_{n0}\begin{bmatrix} \dfrac{1}{1+\omega_{cn}^2\tau_n^2} & \dfrac{\omega_{cn}\tau_n}{1+\omega_{cn}^2\tau_n^2} \\ -\dfrac{\omega_{cn}\tau_n}{1+\omega_{cn}^2\tau_n^2} & \dfrac{1}{1+\omega_{cn}^2\tau_n^2} \end{bmatrix},$$
$$\sigma_p = \sigma_{p0}\begin{bmatrix} \dfrac{1}{1+\omega_{cp}^2\tau_p^2} & \dfrac{\omega_{cp}\tau_p}{1+\omega_{cp}^2\tau_p^2} \\ -\dfrac{\omega_{cp}\tau_p}{1+\omega_{cp}^2\tau_p^2} & \dfrac{1}{1+\omega_{cp}^2\tau_p^2} \end{bmatrix}. \quad (1)$$

Here, σ_{n0} and σ_{p0} are the zero-magnetic field conductivities of n-type and p-type puddles, respectively; τ_n and τ_p are the electrons and holes relaxation times, respectively; whilst ω_{cn}, ω_{cp} are cyclotron frequencies. The zero-field conductivities are given by:[19] $\sigma_{n0} = (2e^2/h)v_F\tau_n\sqrt{\pi n}$ and $\sigma_{p0} = (2e^2/h)$ $v_F\tau_p\sqrt{\pi p}$, where n and p are the carrier concentrations of electrons and holes, respectively. The cyclotron frequency is given by $\omega_{ci} = v_F eB/(\hbar\sqrt{\pi i})$, $i = n, p$. If we consider that the scattering process is mainly due to impurities Coulomb potential, then the relaxation times scale as the square root of the carriers density, i.e., $\tau_{n,p} \propto \sqrt{n,p}$.[8] In this case, we can set $\omega_n\tau_n \equiv \mu_n B$ and $\omega_p\tau_p \equiv \mu_p B$, which are independent of carrier density. The graphene sheet composed of electrons and holes puddles can be regarded as an effective medium with a conductivity tensor σ_e. The conductivity tensor can be calculated using the EMA.[18,20] This approximation assumes electrons and holes puddles as having a compact structure and approximately circular geometry. The expression of the effective conductivity within the EMA is obtained by solving the equation,

$$\sum_i f_i\delta\sigma_i(I - \Gamma\delta\sigma)^{-1} = 0, \quad i = n, p, \quad (2)$$

where $\delta\sigma_i = \sigma_i - \sigma_e$, I is the 2×2 identity matrix and for a planar geometry $\Gamma = -I/2\sigma_{xx}$. Expanding Eq. (2) leads to a couple of nonlinear equations in $\sigma_{e,xx}$ and $\sigma_{e,xy}$, which are the component of the effective conductivity tensor. The other two components are given by $\sigma_{e,yy} = \sigma_{e,xx}$ and $\sigma_{e,yx} = -\sigma_{e,xy}$. The components of the effective conductivity tensor are obtained by numerically solving Eq. (2) and subsequently injecting the obtained values into the FEM model. For our simulations, we assume that $n = p$ and that the relaxation times are the same for electrons and holes, i.e., $\tau_n = \tau_p$, which are independent of the carrier density. In this case, $\mu_n = \mu_p = \mu$ so that $\omega_{c,n,p} = \mu B$ in Eq. (1) and $\sigma_{0n} = \sigma_{0p}$.

Figures 1 and 2 show σ_{xx} and σ_{xy}, respectively, as function of the area fraction of n-type puddles f_n for different values of the magnetic field and for a mobility value of $\mu = 2.3\,T^{-1}$. For these calculations, we set $\sigma_0 = 8e^2/h$.

For a fixed magnetic field, $\sigma_{e,xx}$ reaches a maximum at an area fraction of $f_n = 1/2$. At this value, the component $\sigma_{e,xy}$ vanishes.

Figures 3 and 4 show $\sigma_{e,xx}$ and $\sigma_{e,xy}$ as a function of the applied magnetic field **B** for different values of the electron puddles area fraction. The effective longitudinal conductivity

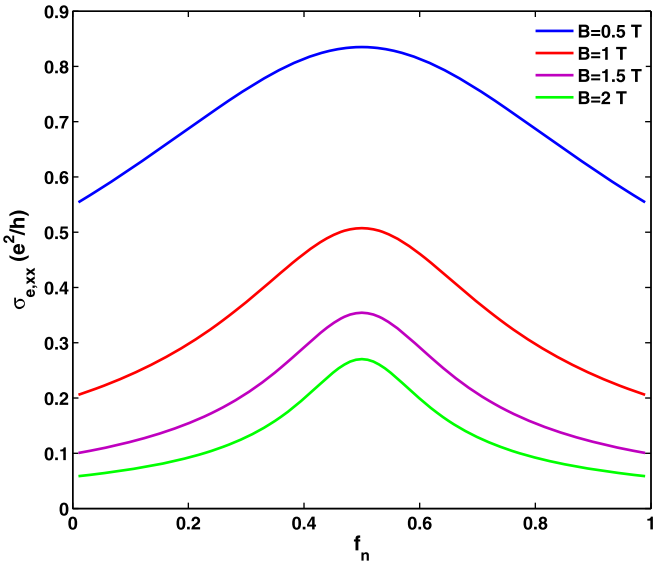

FIG. 1. Plot of the calculated $\sigma_{e,xx}$ as a function of the area fraction f_n for different values of the magnetic field, i.e., B = 0.5 T, 1 T, 1.5 T, and 2 T.

decays as the magnitude of magnetic field is increased. The Hall conductivity vanishes for $f = 1/2$ and saturates at high magnetic field for $f \neq 1/2$.

III. FINITE ELEMENT CALCULATIONS

The FEM analysis is a powerful and predictive tool allowing the simulation of the magnetoresistance of hybrid graphene-metal EMR devices. Previous FEM calculations were performed on thin semiconducting films with metallic inclusions, showing that the MR effect strongly depend on the position, the size of voltage ports,[21] and the contact resistance between the semiconductor and the metal.[22] In the present work, the metal is modelled as a 2D film with the conductivity given by $\sigma_{2D} = \sigma_B * t_m$, where t_m is the thickness of the film and σ_B is the bulk conductivity. Typical values of t_m used in graphene metal contacts are few tens of

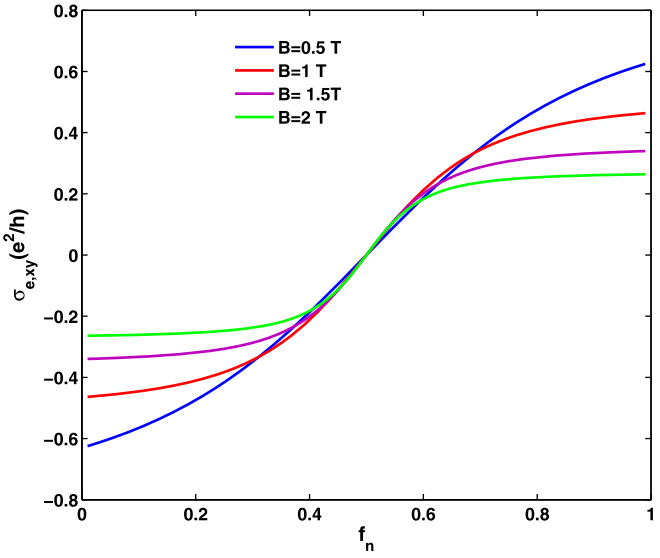

FIG. 2. Plot of the calculated $\sigma_{e,xy}$ as a function of the area fraction f_n for different values of the magnetic field, i.e., B = 0.5 T, 1 T, 1.5 T, and 2 T.

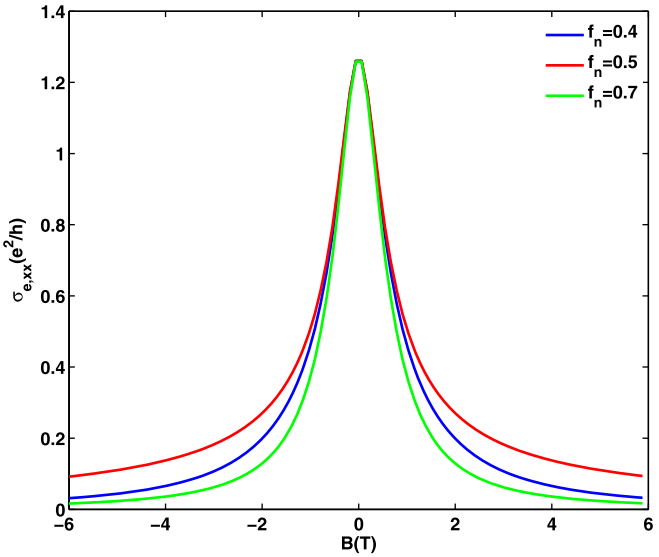

FIG. 3. Calculated $\sigma_{e,xx}$ as a function of the magnetic field for different values of the area fraction $f_n = 0.4$, 0.5, and 0.7.

nanometres. We choose gold as a metal inclusion for our simulations. For an arbitrary geometry, the following equations are solved in two dimensions:

$$\begin{aligned} \nabla \mathbf{J} &= Q_s, \\ \mathbf{J} &= \sigma_e \mathbf{E}, \\ \mathbf{E} &= -\nabla V, \end{aligned} \tag{3}$$

where $\mathbf{J}$ is the current density, Q_s is the current source, and σ_e is the graphene effective conductivity tensor. $\mathbf{E}$ and V are the electric field and the voltage, respectively. The boundary condition for Eqs. (3) satisfies the insulation condition—$\mathbf{n}\cdot\mathbf{J} = \mathbf{0}$, where $\mathbf{n}$ is the normal vector on the boundary. The effective conductivity σ_e is introduced as a parameter after solving Eq. (2) for a given value of the magnetic field and the area fraction of electron (holes) puddles $f_n(f_p)$. The magnetoresistance is defined as

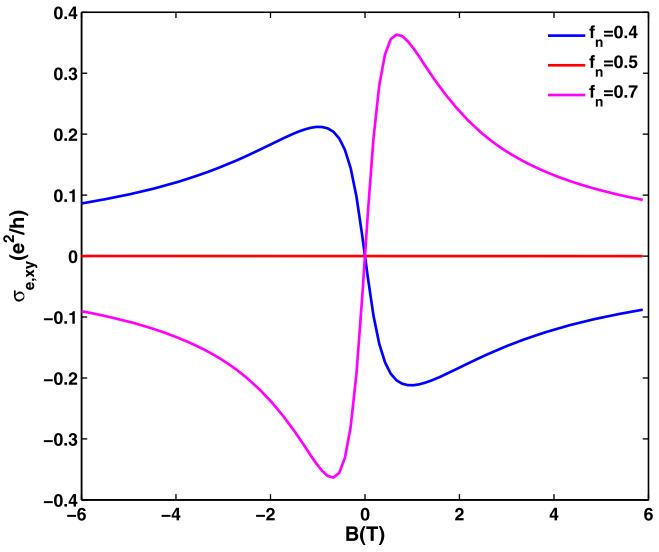

FIG. 4. Calculated $\sigma_{e,xy}$ as a function of the magnetic field for different values of the area fraction $f_n = 0.4$, 0.5, and 0.7.

$$\frac{\Delta R}{R} = \frac{R(B) - R(0)}{R(0)}, \tag{4}$$

where $R(B)$ and $R(0)$ are the resistances between voltage electrodes at fixed and zero magnetic field, respectively.

The metal conductivity tensor has the same form as 1 but with the components given by $\sigma_{m,xx} = \sigma_{m,0}/(1+\mu_m^2 B^2) = \sigma_{m,yy}$ and $\sigma_{m,xy} = \sigma_{m,0}\mu_m B/(1+\mu_m^2 B^2) = -\sigma_{m,xy}$, where $\sigma_{m,0} = \sigma_{2D}$ and μ_m are the metal conductivity and the mobility, respectively.

Here, we will consider two geometries: the circular and the fishbone geometries, using van der Pauw configuration. Surely, other geometries can be considered but these two geometries are chosen for simplicity. The objective here is to show that different geometries produce different magnetoresistance response. FEM simulations are carried out using Comsol Multiphysics[23] with fixed position of the ports and with consideration to contact resistance between graphene and the metal.

IV. RESULTS AND DISCUSSION

The MR not only depends on physical properties of the materials used to build the device, but is strongly dependent on the geometry of the embedded metallic structures on the semiconductor matrice.[12,24] Hewett and Kusmartsev[24] showed that branched geometry led to an enhancement of several orders of magnitudes of the MR compared to the circular geometry for InSb/Au hybrid structure.[12] The MR also depends on the fill factor α which is, for a circular geometry, defined as the ratio $\alpha = r_m/r_G$, where r_m is the radius of the metal inclusion and r_G is the radius of the semiconductor film. Owing to the high graphene mobility, large values of the MR are expected in comparison to other high mobility semiconductors such InSb or InAs. Although 2D electron gas can achieve very high mobilities, graphene offers the advantage of being cheap to produce and simple to process. The MR is expected to be even higher for suspended graphene which shows very high mobility values approaching 200 000 V/cm^2 s.[25]

A. Circular geometry

The circular geometry consists of a circular metal embedded inside a graphene circular sheet of radius $r_G = 2\,\mu$m, the current I is injected at one point and retrieved at another opposite point (−I). The voltage difference ΔV is measured between two opposite probe points as shown in the inset of Figure 5.

The MR effect is akin to classical Hall effect. At zero magnetic field, most of the current flows through the low resistive metallic disc, making the structure short circuited. When applying a magnetic field, the current is forced to flow away from the metallic structure (by the Lorentz force) as the current density acquires a Hall angle with the induced electric field. The current flows in high resistivity region which results in the MR effect. At larger magnetic field, the Hall angle increases (approaching 90°) which forces the current to flow along the edge of the graphene disc resulting in an increase of the length of the current path, and hence

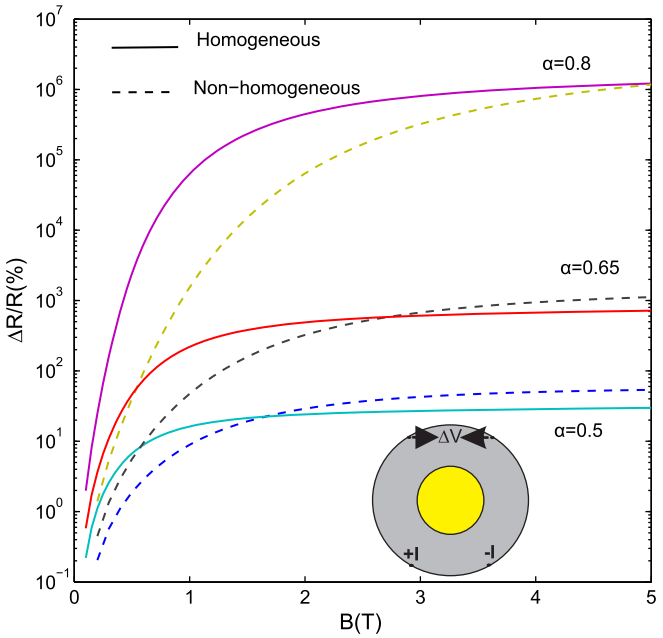

FIG. 5. Plot of the magnetoresistance versus magnetic field for homogenous and non-homogenous graphene, for three values of the fill factor $\alpha = 0.5$, 0.65, and 0.8. For non-homogeneous graphene, the value of $f_n = 0.4$ was used. The structure is shown on the inset where a circular gold shunt is embedded in a circular sheet of graphene. Simulations were performed using a Van der Pauw geometry as indicated.

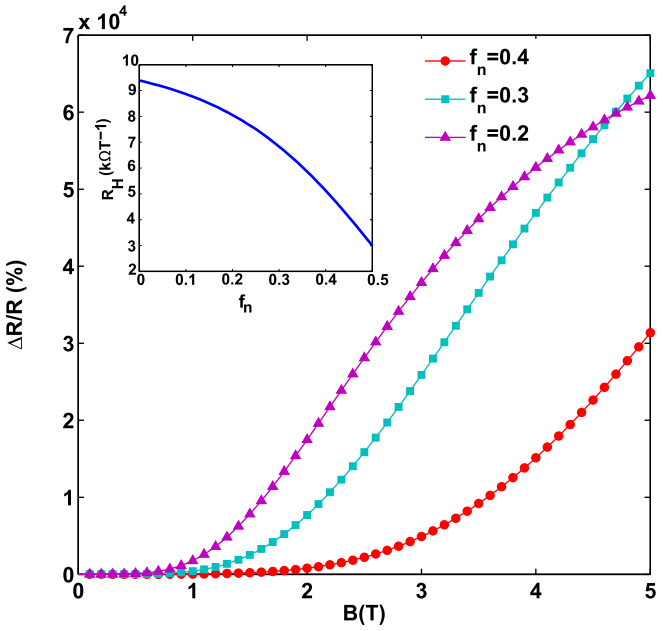

FIG. 6. Magnetoresistance as a function of the applied magnetic field B, of a shunted graphene structure, for three values of the area fraction of electron puddles. The inset shows the Hall coefficient as a function of the puddles area fraction for $B = 0.5$ T.

inducing an enhanced MR. At a fixed magnetic field, changing the dominant puddles landscape from holes to electrons ($f_p \rightarrow 1 - f_p$), results in the current density lines shifting from the right to the left within the structure in a symmetrical manner.

To show the difference between a homogenous graphene made of a single charge carrier type (either p or n) and non-homogeneous graphene made of electron and hole puddles, we perform FEM simulation for both types. The result is displayed in Figure 5 showing $\Delta R/R$ as a function of the magnetic field for homogeneous and non-homogeneous graphene, and for different values of the fill factor. This simulation shows that the presence of electrons and hole puddles weakens the magnetoresistance up to a certain value of the magnetic above which the MR saturates for both homogeneous and non-homogeneous graphene. This saturation is interpreted as follows: as the magnetic field is increased, the current starts to avoid the metal shunt and flows more towards the edges due to the increase of Hall angle. At higher magnetic fields, no current is flowing through the metal shunt (Hall angle approaching 90°) and most of the current flows at the edge of the structure. The transport is limited only by the edges regardless of the value of the magnetic field; therefore, the magnetoresistance saturates.

Figure 6 shows $\Delta R/R$ as a function of the magnetic field for different values of the area fraction of electron puddles. These results were obtained for a metal disc of radius $r = 1.6\,\mu$m. Note that as the problem is symmetrical, the results corresponding to f_n and $1 - f_n$ are identical; hence, we have only considered values of $f_n \leq 1/2$. For this particular geometry and for the range of the magnetic field considered, the MR increases with decreasing electron puddles area fraction. To understand this behavior, we calculate the Hall coefficient R_H for the van der Pauw geometry considered, which is shown in the inset of Figure 6 for $B = 0.5$ T. The Hall coefficient decreases with f_n leading to more charge carriers going through the metal inclusion, which results in a decrease of the MR.

In Figure 7, the simulated MR versus the area fraction f_n is shown, for a magnetic field value of B = 3 T. The MR is increasing with increasing fill factor for all f_n values. For a fixed value of α, the MR produces a maximum at $f_n = 0.58$ and a minimum at $f_n = 0.5$ independent of the fill factor. The

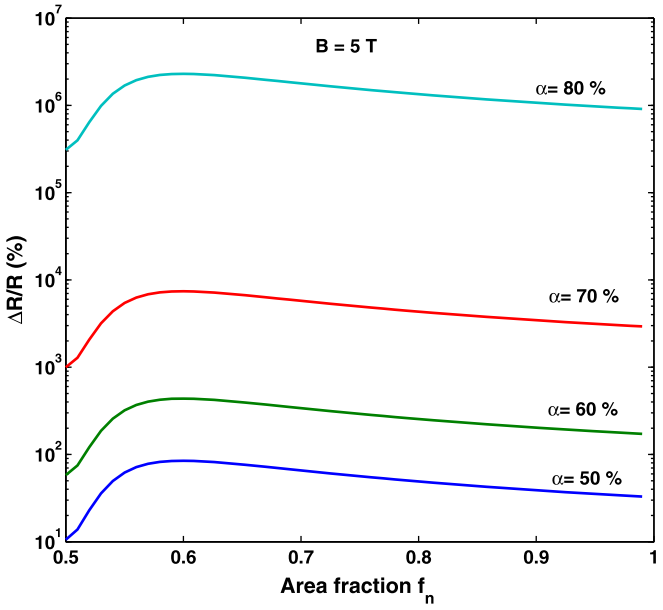

FIG. 7. Dependence of the magnetoresistance on the area fraction f_n for a shunted circular graphene structure, for several values of the fill factor and at a magnetic field value of $B = 5$ T.

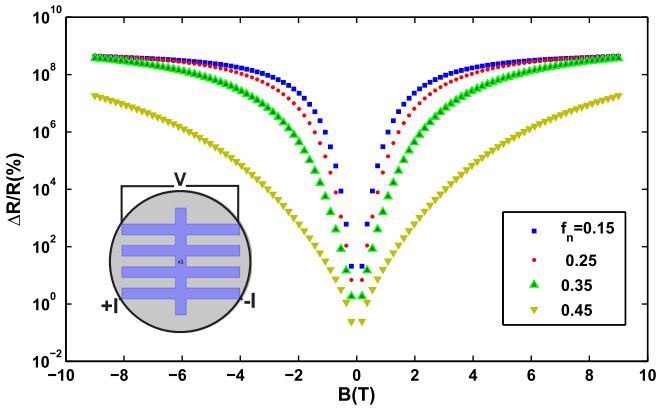

FIG. 8. Dependence of the magnetoresistance on the magnetic field for several values of the area fraction of electron puddles, i.e., 0.15, 0.25, 0.35, and 0.45. The inset shows the metallic fishbone structure embedded in a circular graphene sheet, used in the simulation.

minimum of the MR is attained at $f_n = 0.5$ because the value of the $\sigma_{e,xy}$ vanishes whilst $\sigma_{e,xx}$ reaches its maximum. This makes the structure short, where a large portion of the current flows through the metallic disc as if there were no magnetic field.

B. Fishbone geometry

The fishbone geometry is shown in the inset of Figure 8. The same figure shows the MR as function of the magnetic field for different values of f_n: 0.15, 0.25, 0.35, and 0.45. We can clearly see for this geometry that the MR is strongly dependent on the area fraction of electron and hole puddles. The magnitude of the MR is larger by several orders of magnitude in comparison with the disc geometry. At large magnetic fields, the MR saturates and becomes weakly dependent on f_n as the charge carriers are pushed towards the edges of the structure. For this geometry, the current distribution within the structure in the presence of a magnetic field is more complex compared to the disc structure, but the same mechanism prevails: at zero magnetic field, most of the current flows through the metallic structure whilst at finite **B**, the current is pushed away from it, going through a more resistive path. The strong dependence of the MR of the area fraction f_n is explained by the fact that the Hall coefficient, for the Van der Pauw geometry considered, decreases with f_n (inset of Figure 6). This leads to more charge carriers going through the metal inclusion, which results in a decrease of the MR. It is worth mentioning that there are several geometrical configurations (not shown here), which also result in a very high MR.

So far, we have only considered the situation when $n = p$. If we assume that the Coulomb scattering is the dominating scattering process, then the zero field conductivities $\sigma_{0,n}$ and $\sigma_{0,p}$ are linear in n and p, and if $n \neq p$, these two conductivities are different. In this case, we solve Eq. (2) and perform FEM analysis on the fishbone geometry. In Figure 9, the MR versus the magnetic field is shown for different values of the ratio n/p. It is clear that the MR increases with the ratio n/p. This is resulting from an increase in the Hall resistivity as the ratio n/p is increased as shown in the inset of Figure 9.

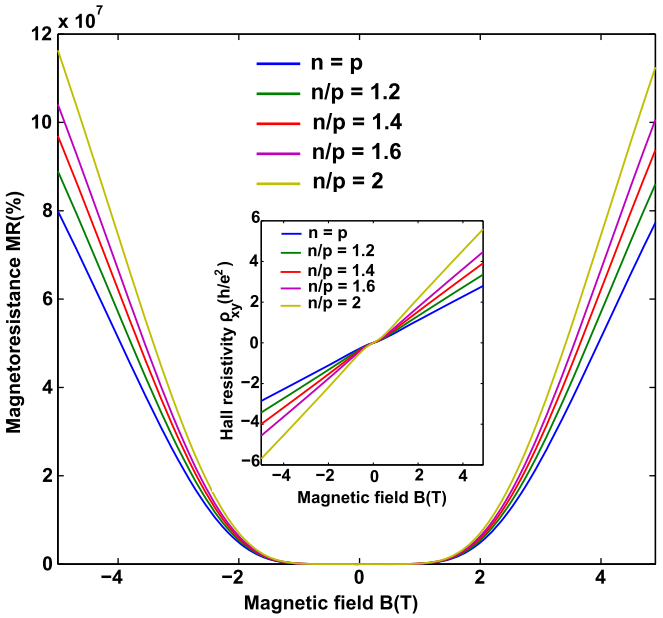

FIG. 9. Dependence of the magnetoresistance on the magnetic field for several values of the ratio n/p, i.e., 1, 1.2, 1.4, 1.6, and 2. The inset shows the Hall resistivity for the same values of n/p.

V. EFFECT OF CONTACT RESISTANCE

It is well known that the contact resistance can have a significant impact on the performance of graphene based devices.[26,27] It is expected that this will also be true for graphene-metal hybrid sensors. In our simulation, we model the contact resistance by inserting a thin layer of width δ, between the fishbone metal shunt and the graphene layer. This contact layer has a magnetic field-independent conductivity tensor given by

$$\sigma_c = \begin{pmatrix} \sigma_{c,xx} & 0 \\ 0 & \sigma_{c,yy} \end{pmatrix}, \tag{5}$$

where $\sigma_{c,xx} = \sigma_{c,yy} = \sigma_c$ are independent of the magnetic field. We choose $\delta = 10\,\text{nm}$ and choose the mesh in the contact sheet to be extremely fine in order ensure numerical accuracy. In Figure 10, we show the MR versus the magnetic field for several values of $\sigma_c\,(1/\Omega)$ and for $f_n = 0.2$. We see that for the fishbone geometry, the MR is strongly dependent on the contact resistance even at large magnetic fields. In the disc geometry, the effect of contact resistance weakens at large magnetic field as the current lines are pushed towards the edge, away from the contact sheet. For the fishbone structure, the strong dependence of the MR at large magnetic fields is explained by the fact that the arms of the structure are very close to the edges of the graphene circular sheet; hence, a large portion of the current still crosses the contact sheet. As the contact conductivity increases and becomes closer to the metal sheet conductivity, the MR becomes weakly dependent on σ_c; in this particular case, this is happening for $\sigma_c \geq 0.01\,\Omega^{-1}$. For practical applications, it is therefore of paramount importance for EMR devices that the contact resistance is minimized.

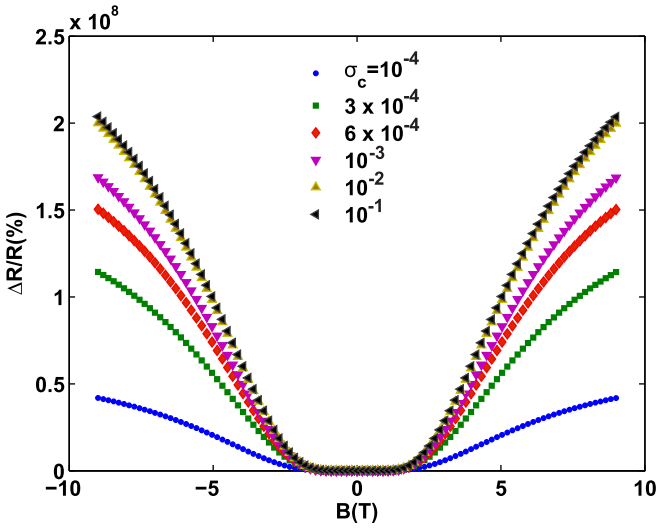

FIG. 10. Dependence of the magnetoresistance on the magnetic field for several values of the contact conductivity σ_c: 10^{-4}, 3×10^{-4}, 6×10^{-4}, 1×10^{-3}, 1×10^{-2}, and 1×10^{-1} $(1/\Omega)$. The simulation was performed for the fishbone geometry.

VI. CONCLUSION

In conclusion, we have applied FEM simulations to investigate the MR on graphene/metal hybrid systems for both homogeneous graphene and non-homogeneous graphene which is made of electron and hole puddles. We considered two geometries: a circular metallic disc and a fishbone metallic structure. It is found that the MR is weaker for non-homogeneous graphene compared with homogenous graphene. It is also found that the MR is strongly dependent on the area fraction of electron and hole puddles. The fishbone geometry shows an enhanced MR in comparison to the circular geometry and exceeds it by several orders of magnitudes. Contact resistance was investigated and it was shown that it can be detrimental to the performance of EMR devices.

[1]K. S. Novoselov *et al.*, Nature **438**, 197 (2005).
[2]Y.-W. Tan, Y. Zhang, K. Bolotin, Y. Zhao, S. Adam, E. H. Hwan, S. D. Sarma, H. L. Stormer, and P. Kim, Phys. Rev. Lett. **99**, 246803 (2007).
[3]S. Cho and M. S. Fuhrer, Phys. Rev. B **77**, 081402(R) (2008).
[4]M. I. Katsnelson and A. K. Geim, Philos. Trans. R. Soc. London, Ser. A **366**, 195204 (2008).
[5]E.-A. Kim and A. H. C. Neto, Eur. Phys. Lett **84**, 57007 (2008).
[6]T. Ando, J. Phys. Soc. Jpn. **75**, 074716 (2006).
[7]K. Nomura and A. MacDonald, Phys. Rev. Lett. **98**, 076602 (2007).
[8]S. Adam, E. H. Hwang, V. M. Galitski, and S. D. Sarma, Proc. Natl. Acad. Sci. U.S.A. **104**, 18392 (2007).
[9]J. Martin, N. Akerman, G. Ulbricht, T. Lohmann, J. H. Smet, K. von Klitzing, and A. A. Yacoby, Nature **4**, 144 (2008).
[10]J. H. Chen, C. Jang, S. Adam, M. S. Fuhrer, E. D. Williams, and M. Ishigami, Nat. Phys. **4**, 377 (2008).
[11]E. H. Hwang, S. Adam, and S. D. Sarma, Phys. Rev. B **76**, 195421 (2007).
[12]S. Solin, T. Thio, D. Hines, and J. Heremans, Science **289**, 1530 (2000).
[13]T. Thio and S. Solin, Appl. Phys. Lett. **72**, 3497 (1998).
[14]C. H. Moller, O. Kronenwerth, D. Grundler, W. Hansen, C. Heyn, and D. Heitmann, Appl. Phys. Lett. **80**, 3988 (2002).
[15]S. Pisana, P. M. Braganca, E. E. Marinero, and B. A. Gurney, Nano Lett. **10**, 341 (2010).
[16]J. Bai, R. Cheng, F. Xiu, L. Liao, M. Wang, A. Shailos, K. L. Wang, Y. Huang, and X. Duan, Nat. Nanotechnol. **5**, 655 (2010).
[17]J. Lu, H. Zhang, W. Shi, Z. Wang, T. Z. Y. Zheng, N. Wang, Z. Tang, and P. Sheng, Nano Lett. **11**, 2973 (2011).
[18]R. P. Tiwari and D. Stroud, Phys. Rev. B **79**, 165408 (2009).
[19]S. D. Sarma, S. Adam, E. H. Hwang, and E. Rossi, Rev. Mod. Phys. **83**, 407 (2011).
[20]D. Stroud, Phys. Rev. B **12**, 3368 (1975).
[21]J. Moussa, L. R. Ram-Mohan, J. Sullivan, T. Zhou, D. R. Hines, and S. A. Solin, Phys. Rev. B **64**, 184410 (2001).
[22]M. Holz, O. Kronenwerth, and D. Grundler, Phys. Rev. B **67**, 195312 (2003).
[23]See www.comsol.com for more information on the FEM package.
[24]T. H. Hewett and F. V. Kusmartsev, Phys. Rev. B **82**, 212404 (2010).
[25]K. Bolotin, K. Sikes, Z. Jiang, M. Klima, G. Fudenberg, J. Hone, P. Kim, and H. Stormer, Solid State Commun. **146**, 351–355 (2008).
[26]S. Russo, M. F. Craciun, M. Yamamoto, A. F. Morpurgo, and S. Tarucha, Physica E (Amsterdam) **42**, 677 (2010).
[27]F. Xia, V. Perebeinos, Y. Lin, Y. Wu, and P. Avouris, Nat. Nanotechnol. **6**, 179 (2011).